

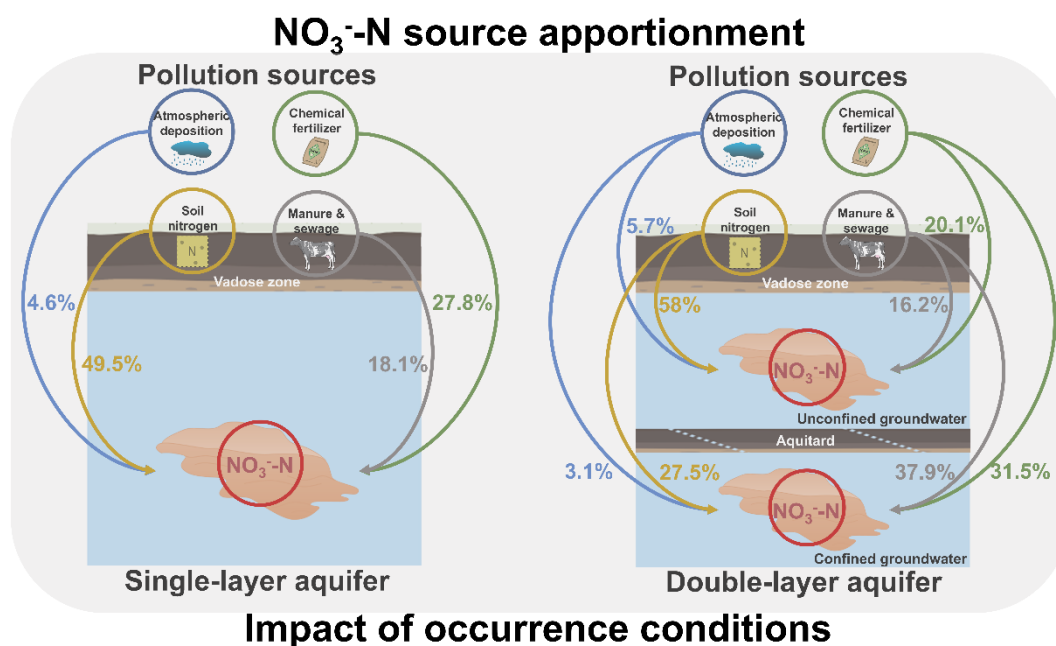


29 for drinking water quality of China ( $\leq 10 \text{ mg N L}^{-1}$ ).  $\text{NO}_3^-$ -N in unconfined  
 30 groundwater predominantly originates from soil nitrogen (58%), with a non-negligible  
 31 contribution from chemical fertilizers.  $\text{NO}_3^-$ -N enrichment in confined groundwater is  
 32 primarily attributed to manure & sewage (37.9%). In addition, ignoring the  
 33 groundwater occurrence conditions leads to marked deviations in the source  
 34 apportionment results derived from both the PCA-APCS-MLR and MixSIAR  
 35 approaches. This study highlights that considering the occurrence conditions is crucial  
 36 for distinguishing the primary sources of  $\text{NO}_3^-$ -N in groundwater, which can enhance  
 37 the accuracy of source apportionment and the effectiveness of management measures.

38 **Keywords:** Groundwater; occurrence conditions;  $\text{NO}_3^-$ -N source apportionment; PCA-  
 39 APCS-MLR; MixSIAR

40

41 **Graphical Abstract**



42

43

44 **Highlights**

- 45 • Elucidated the sources of  $\text{NO}_3^-$ -N in groundwater under different occurrence
- 46 conditions.
- 47 • Soil nitrogen contributes over 50% to the  $\text{NO}_3^-$ -N in the unconfined groundwater.

- 48 •  $\text{NO}_3^-$ -N in confined groundwater mainly originates from manure & sewage.
- 49 • Neglecting occurrence conditions leads to significant deviations in source
- 50 apportionment.

51

## 52 **1. Introduction**

53 Groundwater nitrate-N ( $\text{NO}_3^-$ -N) contamination has persisted for nearly a century  
54 worldwide, emerging as a critical environmental challenge that threatens both human  
55 health and ecological security (Xin et al., 2019). As a highly toxic pollutant,  $\text{NO}_3^-$ -N  
56 poses significant health risks including methemoglobinemia and cancer through  
57 drinking water (Picetti et al., 2022), particularly when its concentration exceeds the  
58 WHO drinking water standard of  $11.3 \text{ mg N L}^{-1}$ . It also causes severe ecological impacts  
59 such as aquatic eutrophication, primarily through groundwater discharge into rivers,  
60 lakes, and coastal waters (Romanelli et al., 2020). The environmental persistence of  
61  $\text{NO}_3^-$ -N is exacerbated by limited natural attenuation in groundwater systems due to  
62 weak denitrification processes, resulting in long-term accumulation of  $\text{NO}_3^-$ -N (Rivett  
63 et al., 2008). The primary sources of  $\text{NO}_3^-$ -N include non-point source pollution from  
64 agricultural activities (fertilizer application and livestock operations) and point source  
65 pollution from industrial effluents and domestic sewage (Xin et al., 2021).  
66 Consequently, the accurate identification and dissection of  $\text{NO}_3^-$ -N pollution sources  
67 are pivotal to the assessment and control of groundwater pollution risks. Despite some  
68 advancements in  $\text{NO}_3^-$ -N source apportionment over the past decades (Yang et al., 2013;  
69 Gibrilla et al., 2020), the majority of studies have overlooked the occurrence conditions  
70 of groundwater. Ignoring this issue can lead to inaccurate source apportionment results,  
71 and consequently affect the scientific nature and effectiveness of groundwater pollution  
72 prevention and control strategies.

73 Current studies on  $\text{NO}_3^-$ -N source apportionment in groundwater predominantly  
74 simplifies complex multi-layer aquifer systems into single-layer models (Yu et al.,  
75 2020). While this simplification facilitates analysis, it introduces substantial limitations

76 due to fundamental differences between unconfined and confined aquifers in terms of  
77 recharge mechanisms, flow paths, hydraulic characteristics, and contaminant transport  
78 behavior (Liang et al., 2017). Unconfined aquifers, characterized by strong connectivity  
79 with surface water, are highly vulnerable to anthropogenic activities (e.g., agricultural  
80 fertilization, industrial effluents, and domestic sewage), allowing contaminants to  
81 readily leach into groundwater through precipitation or surface runoff, resulting in rapid  
82  $\text{NO}_3^-$ -N accumulation that typically reflects recent pollution caused by recent human  
83 activities (Gutiérrez et al., 2018). In contrast, confined aquifers, protected by overlying  
84 aquitards, exhibit slower contaminant migration, with  $\text{NO}_3^-$ -N pollution often  
85 representing legacy effects from historical agricultural practices (Wong et al., 2015). In  
86 addition, the transformation rates of nitrogen components from different pollution  
87 sources vary in aquifers with different occurrence conditions. Unconfined aquifers are  
88 generally aerobic environments, where the mineralization and nitrification of organic  
89 nitrogen occur rapidly, leading to a swift increase in  $\text{NO}_3^-$ -N concentration (Liu et al.,  
90 2022). In contrast, confined aquifers tend to have reducing conditions, which restrict  
91 the nitrogen transformation rate and cause a lag in  $\text{NO}_3^-$ -N formation (Ma et al., 2019).  
92 As a result, the source of  $\text{NO}_3^-$ -N may be mistakenly attributed to other pollution  
93 sources.

94 In recent years, some progress has been made in the identification of  $\text{NO}_3^-$ -N  
95 pollution sources in groundwater through the application of hydrochemical analysis  
96 methods and stable isotope mixing models (Minet et al., 2017; Yu et al., 2022).  
97 Hydrochemical analysis methods mainly include ion ratio methods, hydrochemical  
98 diagram methods, and quantitative hydrochemical analysis methods. Among these,  
99 quantitative hydrochemical analysis is the core, which encompasses models such as the  
100 chemical mass balance (CMB), positive matrix factorization (PMF), and multivariate  
101 statistical models (e.g., principal component analysis and multiple linear regression  
102 analysis). Among these methods, the absolute principal component score-multiple  
103 linear regression (APCS-MLR) method has garnered considerable attention due to its

104 high efficiency and broad applicability (Meng et al., 2018; Ruan et al., 2024). APCS-  
105 MLR can extract key pollution source information by reducing data redundancy  
106 through principal component analysis while retaining the essential characteristics of  
107 major pollution sources. Additionally, APCS-MLR can establish a quantitative  
108 relationship between principal component scores and actual pollutant concentrations  
109 via multiple linear regression, thereby accurately calculating the contribution rates of  
110 various pollution sources. Subsequently, stable isotope techniques have been applied in  
111 the identification of  $\text{NO}_3^-$ -N pollution sources in groundwater. The development of this  
112 technology in groundwater  $\text{NO}_3^-$ -N source apportionment has evolved from the use of  
113 single isotopes ( $\delta^{15}\text{N}$ ) to the combined application of multiple isotopes (both  $\delta^{15}\text{N}$  and  
114  $\delta^{18}\text{O}$ ) (Kellman and Hillaire-Marcel, 2003; Ji et al., 2022). By analyzing the isotopic  
115 compositions of nitrogen ( $\delta^{15}\text{N}$ ) and oxygen ( $\delta^{18}\text{O}$ ) in  $\text{NO}_3^-$ -N, this technique can  
116 effectively distinguish different sources of  $\text{NO}_3^-$ -N pollution in groundwater (such as  
117 agricultural fertilization, domestic sewage, soil nitrogen, and atmospheric deposition)  
118 (Ransom et al., 2016), thereby providing an important supplement to traditional  
119 hydrochemical analysis methods. To further quantify the contribution proportions of  
120 different pollution sources and enhance the accuracy of source identification, the stable  
121 isotope mixing model based on the R language, MixSIAR, has been developed. The  
122 MixSIAR method, by integrating isotope data with prior information (the ranges of  
123 isotopic values and initial estimates of their contributions) on pollution sources, is  
124 capable of quantifying the relative contributions of different pollution sources and  
125 assessing the uncertainty of the results. For example, Mao et al. (2023) used the  
126 MixSIAR method to analyze the distribution of  $\text{NO}_3^-$ -N pollution sources in the  
127 groundwater of Poyang Lake, China, revealing that manure & sewage accounted for  
128 52%, chemical fertilizers for 17%, and soil nitrogen for 21.5% of the pollution sources.  
129 In this study, hydrochemical analysis methods and the MixSIAR method were  
130 employed to comprehensively identify the  $\text{NO}_3^-$ -N pollution sources in groundwater  
131 under different occurrence conditions.

132 To bridge the methodological gap associated with overlooking groundwater  
133 occurrence conditions in  $\text{NO}_3^-$ -N source apportionment and to elucidate the genesis of  
134 “high-nitrogen groundwater” in the Old County groundwater source area, this study  
135 undertook an integrated field sampling and laboratory analysis. Groundwater samples  
136 were collected from 64 wells. Soil, fertilizer, manure, and precipitation samples were  
137 also gathered within the study area. The hydrochemical indicators and isotopic  
138 characteristics of these samples were analyzed. Subsequently, PCA-APCS-MLR and  
139 MixSIAR methods were employed for pollution source apportionment. The objectives  
140 of this study are (1) to quantify the concentration and distribution of  $\text{NO}_3^-$ -N in  
141 groundwater within the study area; (2) to quantitatively identify the sources of  $\text{NO}_3^-$ -N  
142 contamination in groundwater under different occurrence conditions using  
143 hydrochemical analysis and the MixSIAR method; and (3) to clarify distinct  $\text{NO}_3^-$ -N  
144 pollution sources in confined and unconfined groundwater, highlighting the critical role  
145 of occurrence conditions for targeted management. We hypothesize that the primary  
146 sources of  $\text{NO}_3^-$ -N pollution differ significantly between unconfined and confined  
147 groundwater, and neglecting occurrence conditions will introduce a discrepancy in the  
148 results of quantitative  $\text{NO}_3^-$ -N source apportionment. The study aims to provide a more  
149 accurate basis for assessing the risk of  $\text{NO}_3^-$ -N contamination in regional groundwater.

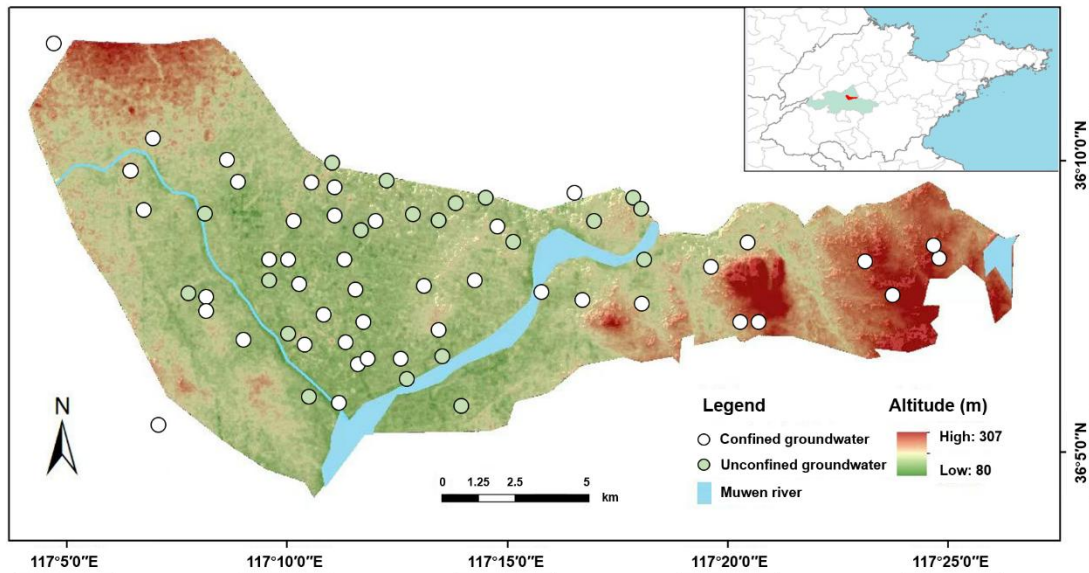
150

## 151 **2. Materials and methods**

### 152 **2.1 Study region**

153 The study area is located on the western edge of the Tai-Lai Basin in the lower  
154 reaches of the Yellow River (Fig.1), to the east of Tai'an urban area ( $117^\circ04'09''\text{E}$ –  
155  $117^\circ26'45''\text{E}$ ,  $36^\circ04'16''\text{N}$ – $36^\circ12'10''\text{N}$ ), with a total area of approximately 220  $\text{km}^2$ .  
156 The topography is characterized as a proluvial and alluvial plain at the foot of Mount  
157 Tai, with an overall terrain slope from the northwest to the southeast. The study area  
158 falls within the temperate continental semi-humid monsoon climate zone, featuring hot  
159 and rainy summers, as well as cold and dry winters. The average annual temperature is

160 12.9°C, and the average annual precipitation is 790.69 mm. Precipitation exhibits  
161 significant spatiotemporal variability, with uneven seasonal distribution and large  
162 interannual fluctuations. The primary aquifer formations in the study area consist of  
163 two types: the Quaternary unconsolidated porous aquifer group and the Cambrian-  
164 Ordovician carbonate rock fracture karst aquifer group. The former is mainly composed  
165 of medium to coarse sand, with recharge primarily from atmospheric precipitation and  
166 infiltration of surface water, and discharge through evaporation, artificial extraction,  
167 replenishment of surface water, and inter-aquifer flow to other aquifers. The latter is  
168 mostly situated beneath the Quaternary strata, with recharge mainly from "skylight"  
169 recharge of Quaternary water and lateral flow recharge from regional bedrock fracture  
170 aquifers, and discharge through artificial extraction, runoff discharge, and upward  
171 replenishment to the Quaternary porous water. The urban population in the study area  
172 is approximately 28,000, with over 85% of the population engaged in agriculture and  
173 animal husbandry.



174  
175 **Fig.1.** Location of the Tailai Basin in lower reaches of the Yellow River and sampling sites in the  
176 study region.

## 177 2.2 Sample collection

178 A total of 64 groundwater samples were collected from the study area. Prior to  
179 sampling, wells were thoroughly flushed, and samples were taken from a depth of more

180 than 0.5 m below the groundwater table. For sealed wells, water stored in the pumping  
181 pipe was completely drained before sampling. After collection, groundwater samples  
182 were filtered through a 0.45  $\mu\text{m}$  membrane filter and stored in 500 mL amber glass  
183 bottles, which were then sealed and transported to the laboratory for refrigeration at  
184 4°C. Groundwater samples intended for isotopic analysis were filtered through a 0.22  
185  $\mu\text{m}$  membrane filter and stored frozen in 50 mL polyethylene bottles. Five atmospheric  
186 precipitation samples were collected using stainless-steel precipitation samplers. For  
187 single-day precipitation events, one complete-event sample was collected, while for  
188 multi-day precipitation events, samples were collected at 24-hour intervals. All  
189 precipitation samples were stored in polyethylene bottles. Five typical fertilizer samples  
190 (including urea and compound fertilizers) were collected based on local farmers'  
191 fertilization practices. Given the difficulty in distinguishing between manure & sewage  
192 pollution sources using  $\delta^{15}\text{N}$  and  $\delta^{18}\text{O}$  isotopes, these two sources were combined into  
193 one category in this study. A total of 10 samples (including cow manure, pig manure,  
194 chicken manure, sheep manure, goose manure, and sewage) were collected. Manure  
195 samples were air-dried for later use, while sewage samples were filtered through a 0.22  
196  $\mu\text{m}$  membrane filter and stored frozen. Additionally, 20 agricultural soil samples were  
197 collected using the plum blossom point layout method. Each sample was composed of  
198 a mixture from 5 to 15 sampling points at a depth of 30 cm, with all sampling points  
199 avoiding fertilized areas. The collected soil samples were thoroughly mixed after  
200 removing roots and gravel and then stored.

### 201 **2.3 Sample Analysis**

202 The concentration of  $\text{NO}_3^-$ -N was determined using the ultraviolet  
203 spectrophotometric method (at 220 nm and 275 nm) following filtration through a 0.45  
204  $\mu\text{m}$  membrane. The concentrations of major ions ( $\text{K}^+$ ,  $\text{Na}^+$ ,  $\text{Ca}^{2+}$ ,  $\text{Mg}^{2+}$ ,  $\text{Cl}^-$ , and  $\text{SO}_4^{2-}$ )  
205 were measured using an ion chromatograph (ICS-3000, Dionex, USA). The separation  
206 was achieved with an IonPac AS23 analytical column and an AG23 guard column,  
207 using a carbonate eluent. The concentration of  $\text{HCO}_3^-$  was determined by acid-base

208 titration with a standardized HCl solution (0.02 M) to a bromocresol green-methyl red  
209 endpoint. All analyses of hydrochemical indicators adhered to standard methods  
210 (Greenberg et al., 2005).

211 In the analysis of isotopic samples,  $\delta^{15}\text{N}$  and  $\delta^{18}\text{O}$  were measured using the azide  
212 reduction method for liquid samples (groundwater, atmospheric precipitation, and  
213 sewage). This involved chemically reducing  $\text{NO}_3^-$ -N in the samples to  $\text{N}_2\text{O}$ , which was  
214 then analyzed using an elemental analyzer coupled with an isotope ratio mass  
215 spectrometer (Vario Isotope Cube - Isoprime, Elementar) to obtain the isotopic values  
216 of  $\delta^{15}\text{N}$  and  $\delta^{18}\text{O}$ . For solid samples (soil, fertilizer, and manure),  $\delta^{15}\text{N}$  and  $\delta^{18}\text{O}$  were  
217 measured using the high-temperature oxidation method. This procedure involved  
218 weighing an appropriate amount of thoroughly ground powder sample, encapsulating  
219 it in a tin cup, and analyzing it using an elemental analyzer coupled with an isotope  
220 ratio mass spectrometer.

## 221 **2.4 Source apportionment methods**

### 222 2.4.1 Hydrochemical analysis method

#### 223 (1) Piper diagram

224 The method used to determine the hydrochemical type of groundwater is the  
225 Schoeller classification method. First, the concentrations of  $\text{K}^+$ ,  $\text{Na}^+$ ,  $\text{Ca}^{2+}$ ,  $\text{Mg}^{2+}$ ,  $\text{HCO}_3^-$ ,  
226  $\text{SO}_4^{2-}$ ,  $\text{Cl}^-$ , and  $\text{NO}_3^-$ -N in groundwater samples, expressed in milligrams per liter (mg  
227  $\text{L}^{-1}$ ), are converted to milliequivalent concentrations (meq  $\text{L}^{-1}$ ). Subsequently, the  
228 milliequivalent percentage of each ion is calculated. Finally, the hydrochemical type is  
229 determined based on the ions with a milliequivalent percentage greater than 25%. The  
230 milliequivalent percentages of cations and anions for all water samples in the water  
231 quality monitoring data are plotted on a Piper diagram.

#### 232 (2) PCA-APCS-MLR

233 Principal component analysis (PCA) was employed to extract the dominant pollution  
234 factors, and the potential sources of groundwater contamination were inferred in  
235 conjunction with hydrochemical indicators:

$$\begin{cases}
\text{PC}_1 = \mu_{11}x_1 + \mu_{12}x_2 + \dots + \mu_{1j}x_j \\
\text{PC}_2 = \mu_{21}x_1 + \mu_{22}x_2 + \dots + \mu_{2j}x_j \\
\vdots \\
\text{PC}_m = \mu_{m1}x_1 + \mu_{m2}x_2 + \dots + \mu_{mj}x_j
\end{cases} \quad (1)$$

237 PC<sub>1</sub>, PC<sub>2</sub>, ..., PC<sub>m</sub> represent the principal components 1, 2, ..., m that can explain the  
238 original indicators. The eigenvalues  $\lambda_m$  ( $m \leq j$ ) of the correlation coefficient matrix are  
239 the variances of PC<sub>m</sub>, and the larger the variance, the greater the contribution to the  
240 principal component.

241 Subsequently, on the basis of PCA, the absolute principal component scores (APCS)  
242 were determined. A multiple linear regression (MLR) was performed with the measured  
243 pollutant concentrations as the dependent variables and the absolute principal  
244 component scores as the independent variables (Thurston and Spengler, 1985). The  
245 pollution contributions of each factor were calculated based on the regression  
246 coefficients, thereby determining the contribution rates of the pollution sources:

$$(A_0)_p = \sum_{j=1}^J S_{pj}(Z_0)_j \quad (2)$$

248  $p$  represents the principal component extracted during the principal component analysis  
249 (PCA) process.  $(A_0)_p$  denotes the absolute principal component score for principal  
250 component  $p$ .  $S_{pj}$  represents the scoring coefficient of indicator  $j$  within principal  
251 component  $p$ .

$$C_j = b_j + \sum_{p=1}^P b_{pj} \times APCS_{ip} \quad (3)$$

253  $C_j$  represents the measured concentration of pollutant  $j$ .  $b_j$  denotes the constant term in  
254 the multiple linear regression analysis.  $b_{pj}$  represents the regression coefficient for  
255 principal component  $p$ .  $b_{pj} \times APCS_{ip}$  indicates the concentration contribution of principal  
256 component  $p$  to pollutant  $j$  in sample  $i$ . The average value of  $b_{pj} \times APCS_{ip}$  represents the  
257 average concentration contribution of principal component  $p$  (the pollution source) to

258 pollutant  $j$ . Finally, by converting the concentration contributions of each pollution  
 259 source into percentages, the contribution rates of the pollution sources can be  
 260 determined.

#### 261 2.4.2 MixSIAR method

262 The principle of the MixSIAR method is to use the Dirichlet distribution as the prior  
 263 distribution and to obtain the posterior distribution characteristics of the contributions,  
 264 such as the mean, variance, and probability density, through the application of Bayes'  
 265 theorem (Moore and Semmens, 2008). Assuming there are  $n$  samples,  $k$  different  
 266 sources, and  $j$  isotopes, the MixSIAR mixing model can be expressed as follows:

$$\begin{aligned}
 267 \quad X_{ij} &= \sum_{k=1}^K P_k (S_{jk} + \varepsilon_{jk}) + v_{ij} \\
 268 \quad S_{jk} &\sim N(\mu_{jk}, \omega_{jk}^2) \\
 269 \quad \varepsilon_{jk} &\sim N(\lambda_{jk}, \tau_{jk}^2) \\
 270 \quad v_{ij} &\sim N(0, \sigma_j^2) \tag{4}
 \end{aligned}$$

271  $X_{ij}$  represents the value of the  $j$  isotope in the  $i$  sample ( $i=1, 2, 3, \dots, N$ ;  $j=1, 2, 3, \dots,$   
 272  $J$ ).  $P_k$  denotes the contribution rate of the  $k$  source ( $k=1, 2, 3, \dots, K$ ), which is predicted  
 273 using the MixSIAR method.  $S_{jk}$  represents the value of the  $j$  isotope from the  $k$  source,  
 274 with a mean of  $\mu_{jk}$  and a variance of  $\omega_{jk}^2$ .  $\varepsilon_{jk}$  represents the enrichment coefficient of the  
 275  $j$  isotope from the  $k$  source, with a mean of  $\lambda_{jk}$  and a variance of  $\tau_{jk}^2$ .  $v_{ij}$  represents the  
 276 residual, with a mean of 0 and a variance of  $\sigma_j^2$ .

#### 277 2.5 Data analysis

278 The stable isotope mixing model used in this study was run in the R package  
 279 MixSIAR (R version x64 4.3.2). Statistical analysis was performed using SPSS 20  
 280 software. To evaluate the linear relationships between hydrochemical parameters, the  
 281 Pearson correlation coefficient ( $r$ ) was calculated. Correlations were considered  
 282 statistically significant at a two-tailed  $p$ -value  $< 0.05$ . The spatial distribution of  $\text{NO}_3^-$ -  
 283 N concentrations was generated using Surfer 15 software, and the cartographic work

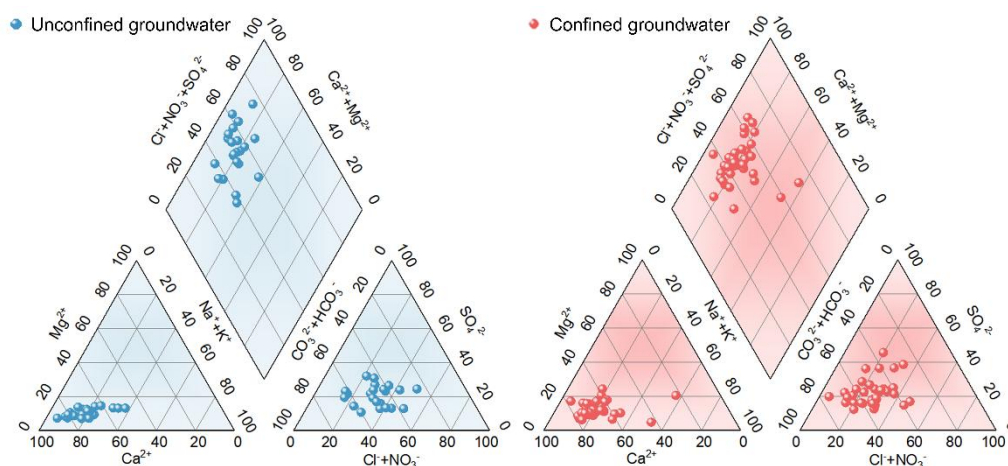
284 was completed with Origin 2020.

285

### 286 3. Results

#### 287 3.1 Characteristics of groundwater NO<sub>3</sub><sup>-</sup>-N pollution

288 The type of groundwater in the study area is predominantly of the Ca-type, with the  
289 molar percentage of Ca<sup>2+</sup> exceeding 50% in most sampling points (Fig.2). In addition,  
290 the groundwater in the study area can be classified into two main types: Cl<sup>-</sup>·NO<sub>3</sub><sup>-</sup>·HCO<sub>3</sub><sup>-</sup>  
291 -Ca<sup>2+</sup> and Cl<sup>-</sup>·NO<sub>3</sub><sup>-</sup>·SO<sub>4</sub><sup>-</sup>-Ca<sup>2+</sup>. Specifically, the Cl<sup>-</sup>·NO<sub>3</sub><sup>-</sup>·HCO<sub>3</sub><sup>-</sup>-Ca<sup>2+</sup> type is primarily  
292 found in karst water, while the Cl<sup>-</sup>·NO<sub>3</sub><sup>-</sup>·SO<sub>4</sub><sup>-</sup>-Ca<sup>2+</sup> type is mainly distributed in pore  
293 water.



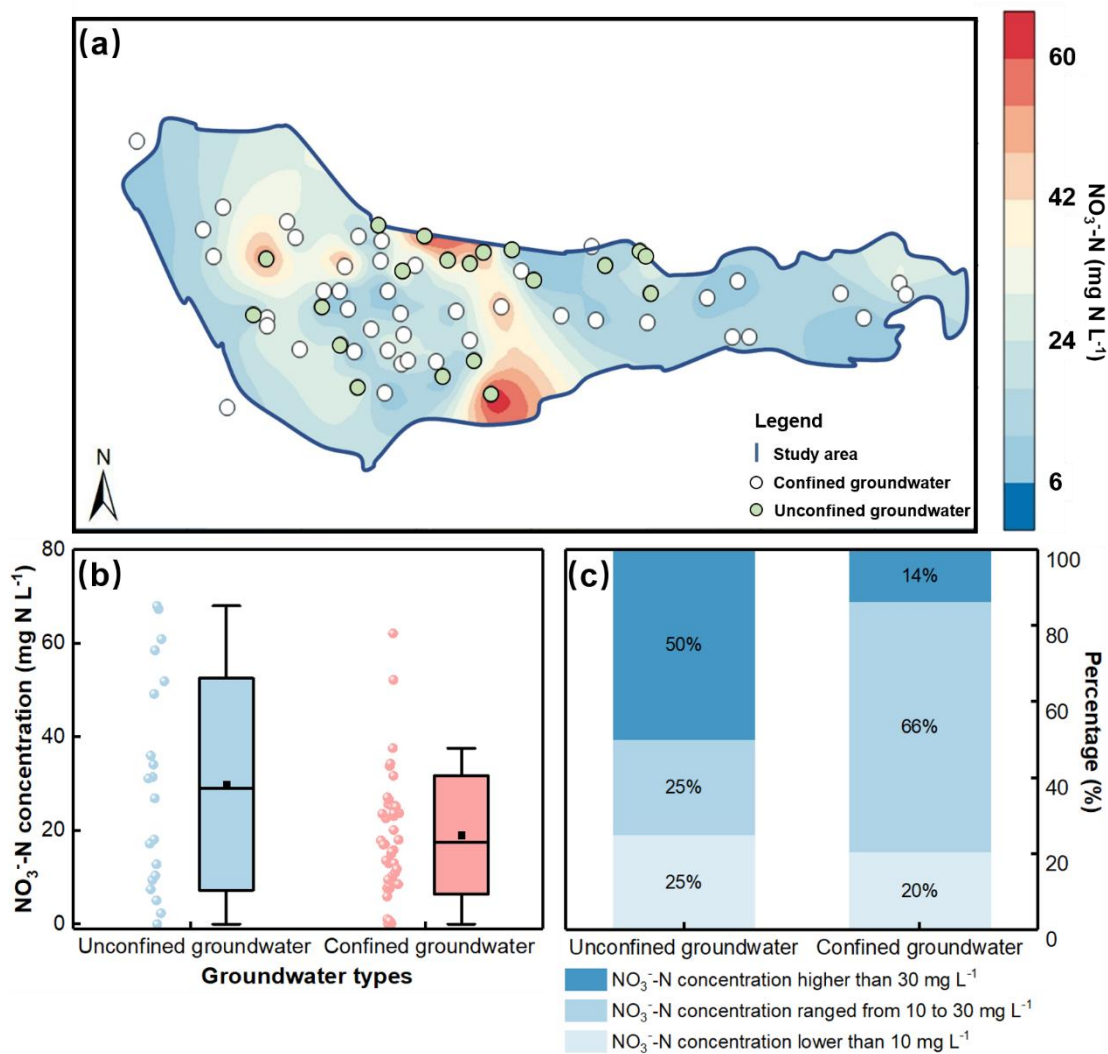
294

295

**Fig.2.** Piper graph illustrating hydrochemical types of groundwater.

296 Kriging interpolation was employed to analyze the spatial distribution of NO<sub>3</sub><sup>-</sup>-N  
297 concentration in the groundwater of the study area. The results indicate that the NO<sub>3</sub><sup>-</sup>-  
298 N concentration in the groundwater ranges from 0 to 68 mg N L<sup>-1</sup>, with an average  
299 concentration of 22.45 mg N L<sup>-1</sup> (Fig.3). Based on the standard for drinking water  
300 quality of China (NO<sub>3</sub><sup>-</sup>-N ≤ 10 mg N L<sup>-1</sup>), the NO<sub>3</sub><sup>-</sup>-N exceedance rate in the study area  
301 is 75%, indicating a relatively severe overall pollution status. Specifically, the NO<sub>3</sub><sup>-</sup>-N  
302 concentration in unconfined groundwater ranges from 0 to 68 mg N L<sup>-1</sup>, with an average  
303 concentration of 29.9 mg N L<sup>-1</sup>, while that in confined groundwater ranges from 0 to  
304 62.1 mg N L<sup>-1</sup>, with an average concentration of 20.1 mg N L<sup>-1</sup>. Additionally, 50% of  
305 the sampling sites in unconfined groundwater and 14% in confined groundwater exceed

306 30 mg N L<sup>-1</sup> (Class V groundwater quality standard of China), suggesting that NO<sub>3</sub><sup>-</sup>-N  
 307 pollution in unconfined groundwater is more severe than that in confined groundwater.  
 308 Spatially, the NO<sub>3</sub><sup>-</sup>-N pollution in the groundwater exhibits significant spatial  
 309 heterogeneity, with the central part of the study area experiencing more severe NO<sub>3</sub><sup>-</sup>-N  
 310 contamination compared to the western and eastern regions.



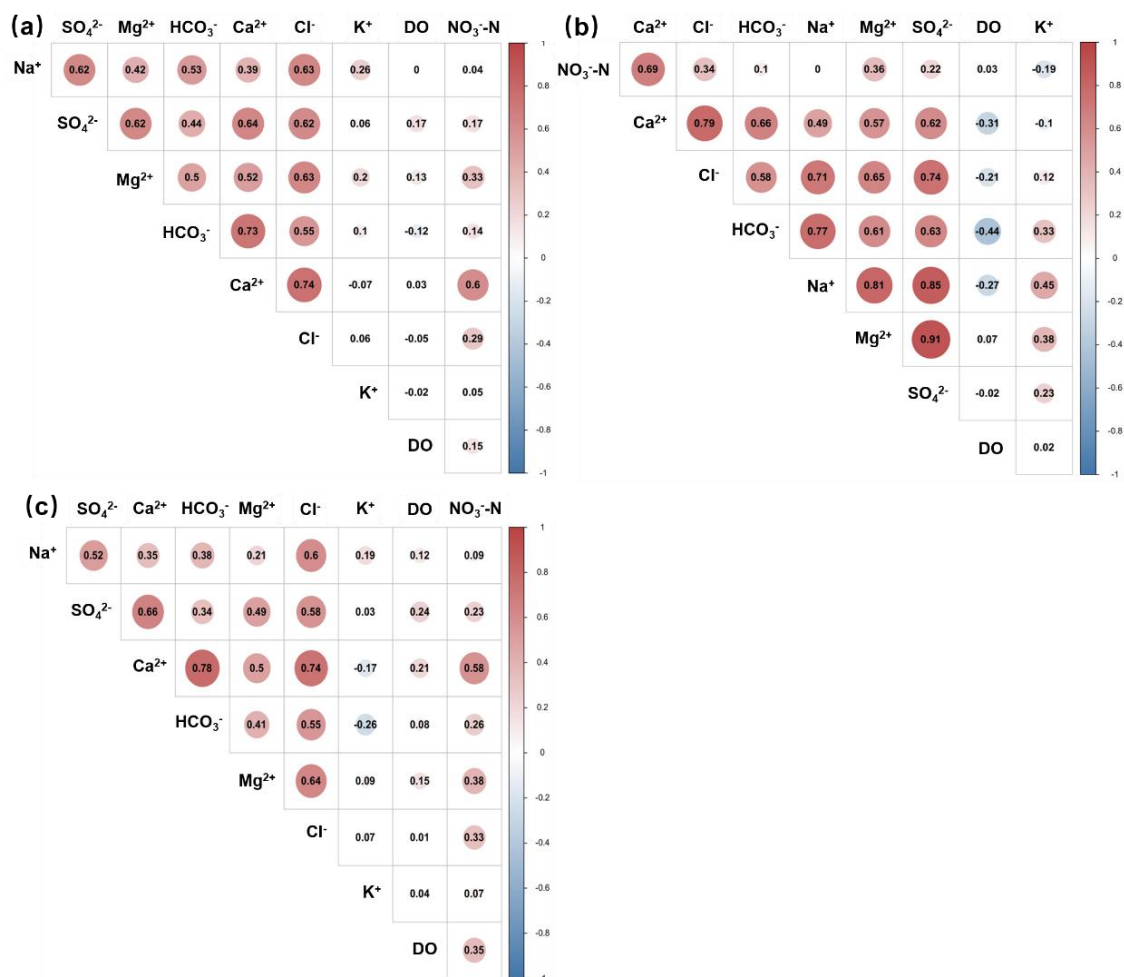
311  
 312 **Fig.3.** (a) Spatial distribution map of NO<sub>3</sub><sup>-</sup>-N concentrations in unconfined and confined  
 313 groundwater of the study region. (b) Boxplot of NO<sub>3</sub><sup>-</sup>-N concentrations. The dot and line represent  
 314 mean value and median. (c) Percentages of NO<sub>3</sub><sup>-</sup>-N concentrations in unconfined groundwater and  
 315 confined groundwater (<10 mg N L<sup>-1</sup>, ranging from 10 to 30 mg N L<sup>-1</sup>, and >30 mg N L<sup>-1</sup>).

### 316 3.2 NO<sub>3</sub><sup>-</sup>-N sources apportionment by PCA-APCS-MLR model

#### 317 3.2.1 Qualitative identification of NO<sub>3</sub><sup>-</sup>-N sources

318 The results of Pearson correlation analysis demonstrate that, in the generalized

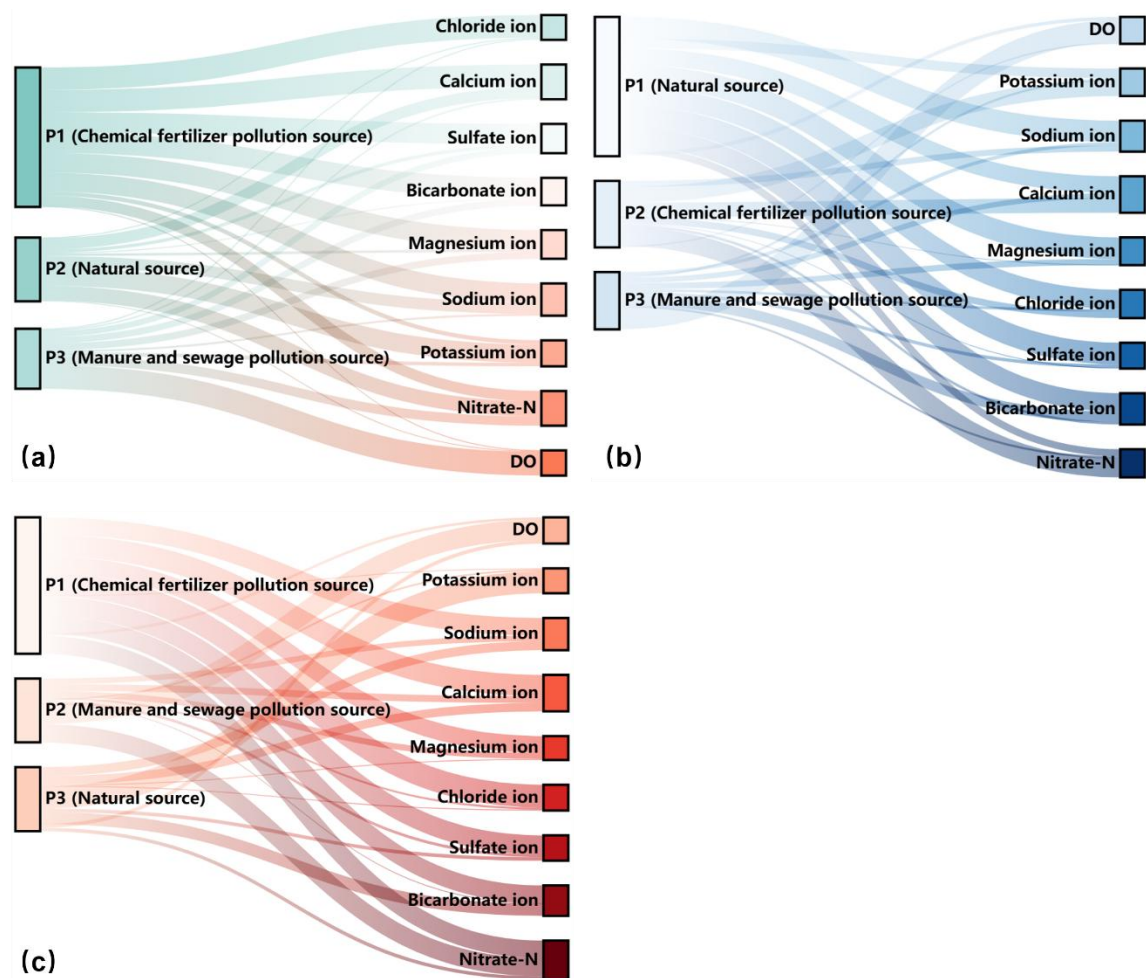
319 single-layer aquifer (refers to the simplified analytical scenario in which groundwater  
 320 samples from both unconfined and confined aquifers are treated as a single  
 321 homogeneous aquifer, without considering differences in occurrence conditions)  
 322 (Fig.4a), there is a strong correlation among the nine hydrochemical indicators. For  
 323 example,  $Mg^{2+}$  is strongly correlated with  $Na^+$ ,  $Ca^{2+}$ ,  $Cl^-$ ,  $SO_4^{2-}$ ,  $HCO_3^-$ , and  $NO_3^-$ , while  
 324  $NO_3^-$  exhibits strong correlations with  $Ca^{2+}$ ,  $Mg^{2+}$ , and  $Cl^-$ . In the actual double-layer  
 325 aquifer (refers to the realistic scenario in which unconfined and confined aquifers are  
 326 analyzed separately, respecting their distinct hydrogeological settings, recharge  
 327 mechanisms, and pollution pathways) (Fig.4b and Fig.4c), the indicators also show  
 328 strong correlations. Specifically,  $Ca^{2+}$  is strongly correlated with  $Na^+$ ,  $Mg^{2+}$ ,  $Cl^-$ ,  $SO_4^{2-}$ ,  
 329  $HCO_3^-$ , and  $NO_3^-$ , and  $NO_3^-$  displays strong correlations with DO,  $Ca^{2+}$ ,  $Mg^{2+}$ , and  $Cl^-$ .  
 330 Therefore, the selected hydrochemical indicators are suitable for principal component  
 331 analysis.



332

333 **Fig.4.** Pearson correlation analysis of different hydrochemical indexes. (a) Generalized single-layer  
334 aquifer. (b) Actual double-layer aquifer (unconfined groundwater). (c) Actual double-layer aquifer  
335 (confined groundwater).

336 Subsequently, we calculated the rotated factor loadings using the varimax rotation  
337 method. The factor loadings reflect the relative importance of each variable in the  
338 principal components. Typically, factor loadings greater than 0.7, between 0.7 and 0.5,  
339 and between 0.5 and 0.3 are defined as strong, moderate, and weak loadings,  
340 respectively. Based on these factors loading results, we identified pollution sources.  
341 The results indicate that, for the generalized single-layer aquifer (Fig.5a), P1 represents  
342 pollution from chemical fertilizers, P2 represents natural sources, and P3 represents  
343 pollution from manure & sewage. For the actual double-layer aquifer, in the unconfined  
344 groundwater (Fig.5b), P1 represents natural sources, P2 represents pollution from  
345 chemical fertilizers, and P3 represents pollution from manure & sewage. In the confined  
346 groundwater (Fig.5c), P1 represents pollution from chemical fertilizers, P2 represents  
347 pollution from manure & sewage, and P3 represents natural sources.



348

349 **Fig.5.** Sankey graph of rotation factor load matrix for hydrochemical indexes. (a) Generalized  
 350 single-layer aquifer. (b) Actual double-layer aquifer (unconfined groundwater). (c) Actual double-  
 351 layer aquifer (confined groundwater).

### 352 3.2.2 Quantitative apportionment of $\text{NO}_3^-$ -N sources

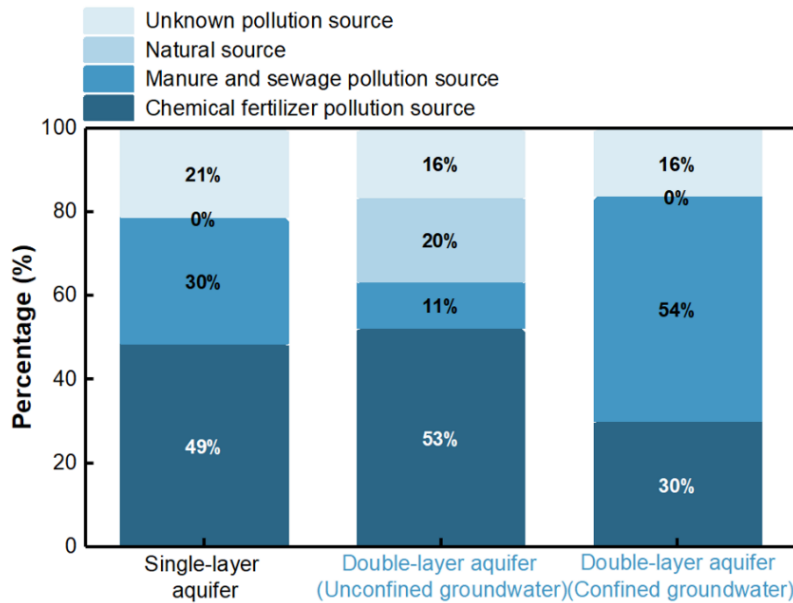
353 Following the qualitative identification of the major pollution sources, the APCS-  
 354 MLR method was employed to quantitatively analyze the pollution sources (Table 1).  
 355 For the generalized single-layer aquifer, the regression equation between  $\text{NO}_3^-$ -N  
 356 concentration and the absolute principal component scores was established as:  
 357  $C=7.231 \times P1-9.786 \times P2+5.655 \times P3-4.45$  ( $R^2=0.789$ ,  $p < 0.01$ ). This regression model  
 358 explains 78.9% of the variation in  $\text{NO}_3^-$ -N concentration, with the remaining 21.1%  
 359 attributable to unknown pollution sources. For the actual double-layer aquifer, in the  
 360 unconfined aquifer, the regression equation between  $\text{NO}_3^-$ -N concentration and the  
 361 absolute principal component scores is:  $C=6.85 \times P1+17.84 \times P2+3.78 \times P3+3.197$

362 ( $R^2=0.838$ ,  $p < 0.01$ ), explaining 83.8% of the variation in  $\text{NO}_3^-$ -N concentration, and  
 363 the remaining 16.2% is attributed to unknown pollution sources. In the confined aquifer,  
 364 the regression equation is:  $C=5.12 \times P1+9.16 \times P2-1.74 \times P3-9.26$  ( $R^2=0.841$ ,  $p < 0.01$ ),  
 365 accounting for 84.1% of the variation in  $\text{NO}_3^-$ -N concentration, with the remaining 15.9%  
 366 attributed to unknown pollution sources.

367 **Table 1.** Multiple regression equation based on APCS-MLR.

Aquifers	Multiple regression equation
Single-layer aquifer	$C=7.231 \times P1-9.786 \times P2+5.655 \times P3-4.45$
Double-layer aquifer (unconfined groundwater)	$C=6.85 \times P1+17.84 \times P2+3.78 \times P3+3.197$
Double-layer aquifer (confined groundwater)	$C=5.12 \times P1+9.16 \times P2-1.74 \times P3-9.26$

368 Furthermore, we calculated the contribution rates of each pollution source using the  
 369 regression equations (Fig.6). For the generalized single-layer aquifer, the contribution  
 370 rates of chemical fertilizers, manure & sewage, natural sources, and unknown pollution  
 371 sources were 48.75%, 30.15%, 0%, and 21.1%, respectively, with chemical fertilizers  
 372 being the dominant pollution source. For the actual double-layer aquifer, in the  
 373 unconfined groundwater, the contribution rates of chemical fertilizers, manure &  
 374 sewage, natural sources, and unknown pollution sources were 52.51%, 11.13%, 20.16%,  
 375 and 16.2%, respectively. In the confined groundwater, the contribution rates were 30.15%  
 376 for chemical fertilizers, 53.95% for manure & sewage, 0% for natural sources, and 15.9%  
 377 for unknown pollution sources. Chemical fertilizers and manure & sewage were  
 378 identified as the primary pollution sources in the unconfined and confined groundwater,  
 379 respectively.



380

381

**Fig.6.** Quantitative apportionment of  $\text{NO}_3^-$ -N source based on the PCA-APCS-MLR method

382

### 3.3 $\text{NO}_3^-$ -N sources apportionment by MixSIAR model

383

#### 3.3.1 Distribution characteristics of $\delta^{15}\text{N}$ and $\delta^{18}\text{O}$ in groundwater

384

We analyzed the  $\delta^{15}\text{N}$  and  $\delta^{18}\text{O}$  values of  $\text{NO}_3^-$ -N in potential pollution sources

385

(atmospheric deposition, soil nitrogen, chemical fertilizers, and manure & sewage) as

386

well as in groundwater within the study area. The results of the  $\delta^{15}\text{N}$  and  $\delta^{18}\text{O}$  values

387

for the potential pollution sources are presented in the Supplementary data (S1). The

388

$\delta^{15}\text{N}$  and  $\delta^{18}\text{O}$  values of  $\text{NO}_3^-$ -N in groundwater within the study area are shown in

389

Fig.7. For the generalized single-layer aquifer, the  $\delta^{15}\text{N}$  values range from 2.8‰ to

390

29.29‰, with an average of 9.85‰, while the  $\delta^{18}\text{O}$  values range from -0.85‰ to

391

15.12‰, with an average of 4.42‰. For the actual double-layer aquifer, the average

392

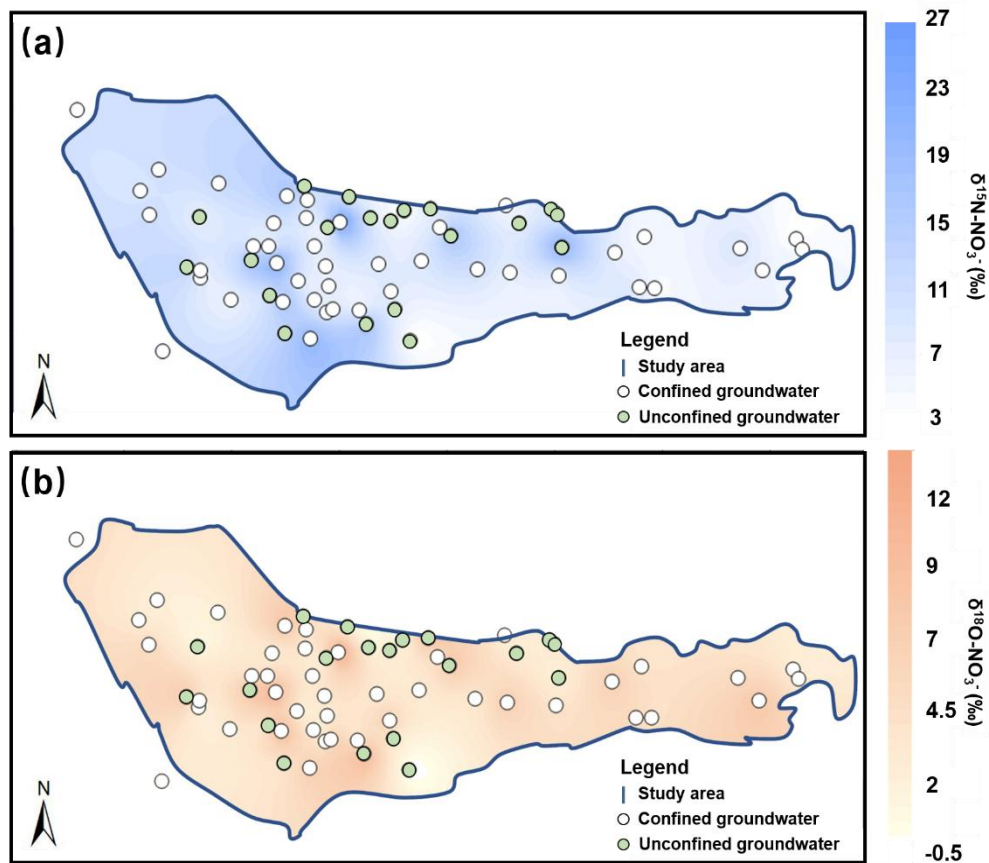
$\delta^{15}\text{N}$  and  $\delta^{18}\text{O}$  values in unconfined groundwater are 10.16‰ and 3.93‰, respectively,

393

and in confined groundwater, the average  $\delta^{15}\text{N}$  and  $\delta^{18}\text{O}$  values are 9.71‰ and 4.6‰,

394

respectively.



395  
396 **Fig.7.** Spatial distribution of  $\delta^{15}\text{N-NO}_3^-$  (a) and  $\delta^{18}\text{O-NO}_3^-$  (b) in the groundwater

397 **3.3.2 Qualitative identification of  $\text{NO}_3^-$ -N sources**

398 The  $\text{NO}_3^-$ -N in the groundwater of the study area originates from multiple nitrogen  
 399 pollution sources. Given the distinct isotopic signatures of  $\delta^{15}\text{N}$  and  $\delta^{18}\text{O}$  of  $\text{NO}_3^-$ -N  
 400 from different sources, qualitative identification of groundwater  $\text{NO}_3^-$ -N sources can be  
 401 achieved based on the characteristic ranges of these dual isotopes. As shown in Fig.8,  
 402 the majority of the  $\delta^{15}\text{N}$  and  $\delta^{18}\text{O}$  values in groundwater locate within the characteristic  
 403 ranges of chemical fertilizers, soil nitrogen, and manure & sewage. This indicates that  
 404 the  $\text{NO}_3^-$ -N in the groundwater of the study area is primarily derived from these three  
 405 pollution sources.

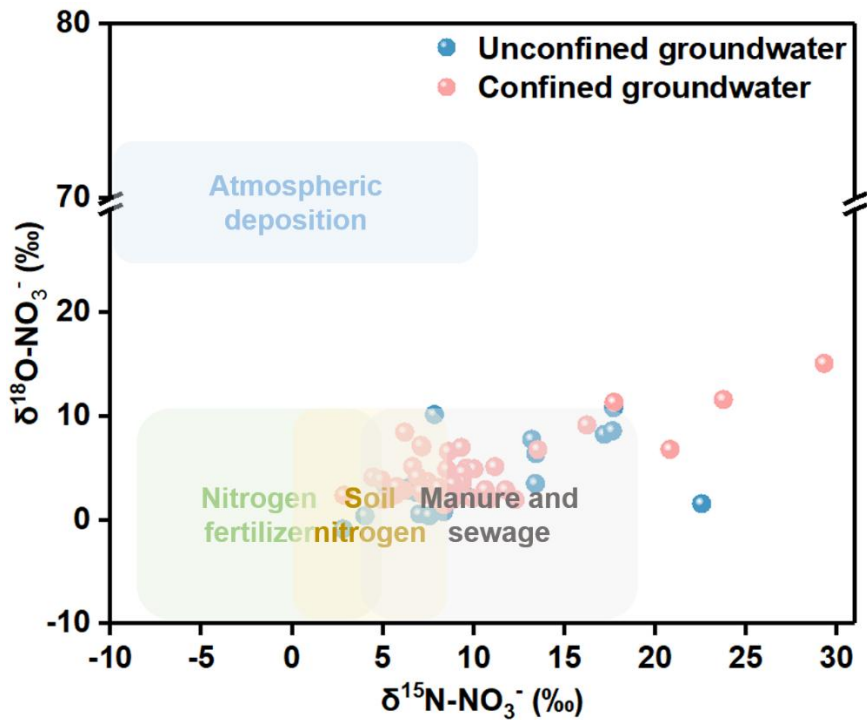
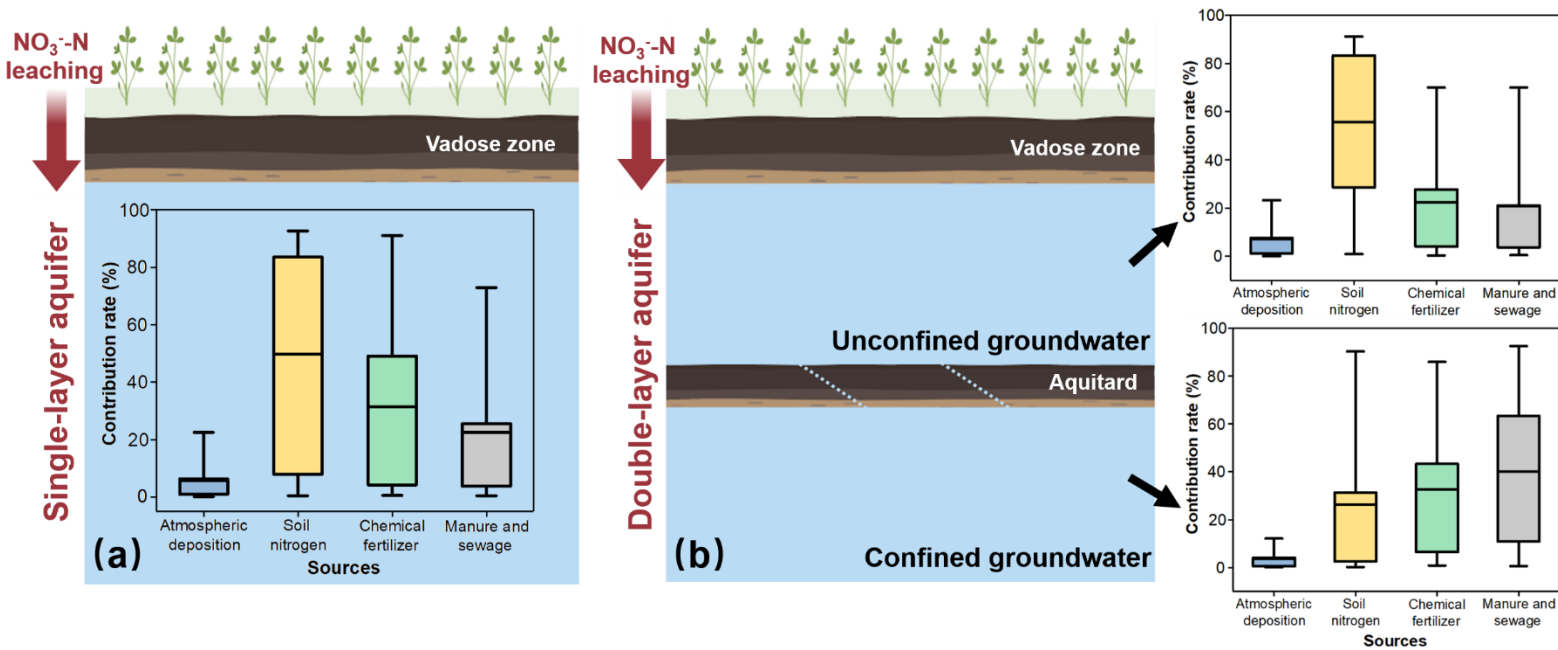


Fig.8. Isotopic ratio plot of  $\delta^{15}\text{N}$  and  $\delta^{18}\text{O}$  of  $\text{NO}_3^-$ -N in Groundwater

### 3.3.3 Quantitative apportionment of $\text{NO}_3^-$ -N sources

The  $\delta^{15}\text{N}$  and  $\delta^{18}\text{O}$  values of groundwater samples, as well as the mean values and standard deviations of  $\delta^{15}\text{N}$  and  $\delta^{18}\text{O}$  for potential pollution sources, were used as known parameters and input into the MixSIAR method. To account for potential errors caused by isotopic fractionation, we calculated the fractionation coefficients for  $\delta^{15}\text{N}$  and  $\delta^{18}\text{O}$  of different pollution sources (Supplementary data, S2) and incorporated these coefficients into the MixSIAR model. Ultimately, by treating the contribution rates of different pollution sources as random variables, we established probabilistic distribution equations for pollution source contributions using the MixSIAR model, thereby determining the extent to which each pollution source contributes to  $\text{NO}_3^-$ -N pollution in groundwater. The results indicate that, for the generalized single-layer aquifer (Fig.9a), the contribution rates of atmospheric deposition, soil nitrogen, chemical fertilizers, and manure & sewage to  $\text{NO}_3^-$ -N pollution are 4.6%, 49.5%, 27.8%, and 18.1%, respectively. For the actual double-layer aquifer (Fig.9b), in the unconfined groundwater, the contribution rates of atmospheric deposition, soil nitrogen, chemical fertilizers, and manure & sewage to  $\text{NO}_3^-$ -N pollution are 5.7%, 58%, 20.1%, and

424 16.2%, respectively. In the confined groundwater, the contribution rates of these four  
 425 pollution sources are 3.1%, 27.5%, 31.5%, and 37.9%, respectively.



426 **Fig.9.** Quantitative apportionment of  $\text{NO}_3^-$ -N source based on the MixSIAR method. (a)  
 427 Generalized single-layer aquifer. (b) Actual double-layer aquifer.

428

#### 429 4. Discussion

430 We employed both the PCA-APCS-MLR method and the MixSIAR method to  
 431 quantitatively identify the sources of  $\text{NO}_3^-$ -N in groundwater under different occurrence  
 432 conditions. For the PCA-APCS-MLR analysis, different ions exhibit varying loading  
 433 strengths in each principal component. Therefore, through hydrochemical analysis and  
 434 statistical methods, we can calculate and infer the type of pollution source represented  
 435 by each principal component. For example, in unconfined groundwater,  $\text{Na}^+$ ,  $\text{Ca}^{2+}$ ,  
 436  $\text{Mg}^{2+}$ ,  $\text{HCO}_3^-$ ,  $\text{SO}_4^{2-}$ , and  $\text{Cl}^-$  have strong loadings in P1. These ions are all major ions  
 437 in groundwater, and their average concentrations are relatively low. Moreover,  
 438 correlation analysis results show that the concentration of  $\text{NO}_3^-$ -N has very low  
 439 correlation with the concentrations of  $\text{Na}^+$ ,  $\text{Mg}^{2+}$ ,  $\text{HCO}_3^-$ ,  $\text{SO}_4^{2-}$ , and  $\text{Cl}^-$ , indicating that  
 440  $\text{NO}_3^-$ -N does not originate from the same source as these ions (Yu et al., 2022). Thus,  
 441 it is demonstrated that P1 represents a natural source. In P2,  $\text{Ca}^{2+}$  and  $\text{NO}_3^-$ -N have

442 strong loadings. The correlation results (Fig.4) indicate a significant positive correlation  
443 between  $\text{Ca}^{2+}$  and  $\text{NO}_3^-$ -N, suggesting that  $\text{Ca}^{2+}$  originates from anthropogenic pollution.  
444 Because  $\text{Ca}^{2+}$  is required in the cultivation of tomatoes and cucumbers (the main crop  
445 types in the study area), and the extensive use of calcium fertilizers during the  
446 application of base fertilizers and top-dressing fertilizers also increases the  
447 concentration of  $\text{Ca}^{2+}$  in groundwater (Schot and Wassen, 1993). Therefore, P2  
448 primarily represents the pollution source from chemical fertilizers. In P3, DO has a  
449 strong loading. Since the oxidation and decomposition of organic matter require a large  
450 amount of DO (Díaz-Cruz and Barceló, 2008), the strong loading of DO is associated  
451 with organic pollution of groundwater (such as from manure & sewage). Thus, P3  
452 mainly represents the pollution sources of manure & sewage. After determining the  
453 pollution sources represented by each principal component using the above methods,  
454 we can calculate the contribution rate of each pollution source using regression  
455 equations. The PCA-APCS-MLR method has the advantages of being rapid and  
456 convenient, but it has the disadvantage of being unable to further identify soil nitrogen  
457 as a pollution source. Accurately apportioning soil-derived  $\text{NO}_3^-$ -N is particularly  
458 challenging for hydrochemical-based methods due to the overlapping ionic signatures  
459 between soil nitrogen and the leaching of synthetic fertilizers or organic wastes (Yu et  
460 al., 2022). To compensate for this limitation, the MixSIAR method was further  
461 employed to analyze the sources of pollution. We identified soil nitrogen as another  
462 important source of  $\text{NO}_3^-$ -N in groundwater. Additionally, we incorporated isotope  
463 fractionation coefficients into the MixSIAR model. Because  $\text{NO}_3^-$ -N from different  
464 sources (atmospheric deposition, soil nitrogen, chemical fertilizers, and manure &  
465 sewage) has distinct isotopic signatures, and isotopic fractionation occurs during the  
466 transport and transformation processes of nitrogen in the groundwater system (such as  
467 ammonification and nitrification), leading to changes in the  $\delta^{15}\text{N}$  and  $\delta^{18}\text{O}$  values of  
468  $\text{NO}_3^-$ -N (Shu et al., 2024). Our MixSIAR model incorporated fractionation factors of  
469 specific nitrogen transformation processes. This approach, essential for reliable

470 quantification, aligns with established practice in  $\text{NO}_3^-$ -N source apportionment studies,  
471 where such constraints are proven to substantially reduce uncertainty (Wang et al.,  
472 2023).

473 In this study, the PCA-APCS-MLR method identified chemical fertilizers as the  
474 primary source of  $\text{NO}_3^-$ -N in unconfined groundwater and manure & sewage as the  
475 main sources of  $\text{NO}_3^-$ -N in confined groundwater. The MixSIAR method further  
476 revealed that soil nitrogen is a dominant pollution source for unconfined groundwater,  
477 with a higher contribution rate than that of chemical fertilizers. The identification of  
478 soil nitrogen as a major contributor in the unconfined groundwater is significant.  
479 Legacy soil nitrogen constitutes a dominant source in the unconfined groundwater, a  
480 finding that shifts the pollution focus from direct fertilizer inputs to cumulative soil  
481 nitrogen pools. This result is consistent with previous  $\text{NO}_3^-$ -N source studies conducted  
482 in other regions (Cui et al., 2023). The findings for unconfined groundwater can be  
483 attributed to the extensive use of chemical fertilizers in agricultural production (Hao et  
484 al., 2025). Nitrogen from these fertilizers can directly leach into the unconfined  
485 groundwater, causing  $\text{NO}_3^-$ -N pollution (Xie et al., 2025). Additionally, excess nitrogen  
486 accumulates in the soil and vadose zone, where it is transformed from organic nitrogen  
487 to  $\text{NH}_4^+$ -N and then to  $\text{NO}_3^-$ -N under the action of soil microorganisms (Liu et al., 2023).  
488 While  $\text{NH}_4^+$ -N can be adsorbed and immobilized by the soil,  $\text{NO}_3^-$ -N can leach into the  
489 deeper vadose zone and aquifer through atmospheric precipitation or agricultural  
490 irrigation, directly contaminating unconfined groundwater (Wan et al., 2024). This  
491 process underscores the phenomenon of the soil and vadose zone as a dynamic  
492 “nitrogen reactor and buffer”. Similar delayed release mechanisms from legacy  
493 nitrogen stored in thick unsaturated zones have been documented in arid regions (Li et  
494 al., 2025), indicating that the risk of groundwater contamination may persist long after  
495 surface inputs are reduced. Thus, in assessing the sources of  $\text{NO}_3^-$ -N pollution in  
496 regional groundwater, it is crucial not only to focus on the application rates of chemical  
497 fertilizers but also to pay attention to the storage of nitrogen in the soil and vadose zone.

498 These accumulated nitrogen compounds can continuously leach into unconfined  
499 groundwater under external disturbances (such as irrigation or precipitation), leading to  
500 persistent contamination (Niu et al., 2022). Therefore, it is essential to guide local  
501 farmers in implementing surface management practices (such as the use of chemical  
502 fertilizers and the application of manure) to enforce optimal agricultural irrigation  
503 policies, including reducing irrigation frequency, to delay the transport of stored  
504 nitrogen in soil to groundwater. For confined groundwater, the MixSIAR method  
505 confirmed that manure & sewage is the major source of  $\text{NO}_3^-$ -N. Generally, the nitrogen  
506 in manure & sewage primarily exists in the form of large molecules. These complex  
507 nitrogen compounds are difficult to degrade microbially or transform chemically in a  
508 short period, leading to their long-term persistence in the environment. These pollutants  
509 can enter surface water bodies through surface runoff or infiltration and then gradually  
510 transport to deeper aquifers via the interflow recharge process between unconfined and  
511 confined aquifers, resulting in persistent contamination (McDonough et al., 2022). This  
512 may highlight a potential mechanism for sustained  $\text{NO}_3^-$ -N pollution in confined  
513 systems, which can be attributed to manure & sewage sources transported via aquifer  
514 exchange, providing a continuous input of recalcitrant nitrogen that gradually  
515 accumulates in this zone (Zhang et al., 2026). Therefore, for the prevention and control  
516 of  $\text{NO}_3^-$ -N pollution in confined groundwater, it is crucial to focus on the source control  
517 of manure & sewage to block the migration pathways of pollutants and mitigate their  
518 long-term impacts.

519 This study assessed the discrepancy in source apportionment of  $\text{NO}_3^-$ -N in  
520 groundwater obtained under different groundwater occurrence conditions. This  
521 discrepancy can be attributed to two main factors. First, the sources and recharge  
522 mechanisms of groundwater in unconfined and confined aquifers differ significantly  
523 (Liu et al., 2025), leading to distinct isotopic compositions and characteristic values.  
524 For example, the isotopic signature of a pollution source in an unconfined aquifer may  
525 resemble that of another source in a confined aquifer. Such overlapping isotopic signals

526 can lead to ambiguous source identification. However, previous studies often fail to  
527 explicitly distinguish between groundwater occurrence conditions, and instead rely on  
528 land-use as a primary proxy for pollution source identification (Yu et al., 2020). When  
529 mixed calculations are performed without considering the actual occurrence conditions,  
530 the isotopic differences are obscured, which may lead to an underestimation or  
531 overestimation of pollution source contributions to groundwater. Second, the migration  
532 and transformation capacities of nitrogen vary among different geological strata.  
533 Hydrogeological conditions can influence the intensity of biogeochemical processes  
534 such as ammonification, nitrification, denitrification (Dai et al., 2023), and adsorption  
535 (Huang et al., 2022; Li et al., 2023), which further alter  $\text{NO}_3^-$ -N concentrations and  
536 isotopic signatures. This ultimately affects the accuracy and reliability of pollution  
537 source apportionment. Consequently, effective management of  $\text{NO}_3^-$ -N in groundwater  
538 systems requires policy interventions tailored to specific groundwater occurrence  
539 conditions. In unconfined groundwater, which is highly vulnerable to surface-derived  
540 inputs, management should prioritize agricultural best practices such as optimized  
541 irrigation scheduling — reducing both frequency and volume of irrigation — coupled  
542 with the promotion of slow-release or stabilized nitrogen fertilizers. These measures  
543 can significantly decrease the rapid leaching of soil nitrogen pools, thereby mitigating  
544 short-term, large-scale pulses of  $\text{NO}_3^-$ -N into groundwater. Besides, the confined  
545 groundwater, often affected by legacy pollution, requires long-term strategies focused  
546 on source control. This includes stricter regulation and monitoring of manure storage  
547 facilities, improved wastewater treatment infrastructure, and the implementation of  
548 containment systems to prevent leaching from historical contamination hotspots. Given  
549 the limited attenuation capacity and persistent nature of  $\text{NO}_3^-$ -N in confined  
550 groundwater, remediation efforts may also need to consider engineered attenuation or  
551 pump-and-treat systems in severely affected zones. Future research should integrate  
552 reactive-transport modeling with isotopic mixing models to better capture the dynamic

553 behavior of nitrogen in dual-layer aquifer systems and to further reduce uncertainty in  
554 source apportionment under varying hydrogeological conditions.

555

## 556 **5. Conclusion**

557 The study quantitatively analyzed the pollution sources of  $\text{NO}_3^-$ -N in groundwater  
558 under different occurrence conditions using PCA-APCS-MLR and MixSIAR methods.  
559 The results showed that the groundwater  $\text{NO}_3^-$ -N concentration in the study area ranged  
560 from 0 to 68 mg N L<sup>-1</sup>, with an exceedance rate of 75%. The  $\text{NO}_3^-$ -N pollution in  
561 unconfined groundwater (average concentration 29.9 mg N L<sup>-1</sup>) was more severe than  
562 that in confined groundwater (average concentration 20.1 mg N L<sup>-1</sup>).  $\text{NO}_3^-$ -N in  
563 unconfined groundwater predominantly originates from soil nitrogen (58%), with a  
564 non-negligible contribution from chemical fertilizers. Therefore, it is necessary to focus  
565 on the storage of nitrogen in the soil and improve agricultural irrigation practices to  
566 prevent rapid infiltration of  $\text{NO}_3^-$ -N into unconfined groundwater, which could lead to  
567 persistent contamination.  $\text{NO}_3^-$ -N enrichment in confined groundwater is primarily  
568 attributed to manure & sewage (37.9%). Regulations and infrastructure for the  
569 treatment and disposal of domestic sewage and livestock waste should be strengthened  
570 to prevent their extensive accumulation in confined groundwater. Moreover, ignoring  
571 the groundwater occurrence conditions leads to marked deviations in the source  
572 apportionment results. Pollution source identification and control policies for  
573 groundwater must explicitly distinguish between unconfined and confined groundwater.

574

## 575 **Acknowledgments**

576 This work was supported by the National Key Research and Development Program  
577 of China (No. 2024YFC3213900), the National Natural Science Foundation of China  
578 (No. 42422207 and No. 42507105).

579

580 **CRedit authorship contribution statement**

581 **Y L:** Writing – review & editing, Writing – original draft, Visualization, Methodology,  
582 Investigation, Formal analysis, Data curation, Conceptualization.

583 **J L:** Writing – review & editing, Supervision, Methodology, Conceptualization.

584 **YJ W:** Writing – review & editing, Supervision, Methodology, Conceptualization.

585 **ZY Z:** Visualization, Investigation, Methodology, Conceptualization.

586 **XL Z:** Supervision, Conceptualization.

587 **TY Z:** Writing – review & editing, Supervision, Resources, Methodology, Investigation,  
588 Conceptualization, Funding acquisition.

589

590 **Declaration of competing interest**

591 The authors declare that they have no known competing financial interests or  
592 personal relationships that could have appeared to influence the work reported in this  
593 paper.

594

595 **Data availability statement**

596 The data of this study can be found in Liu (2025), “Data Availability for HESS”,  
597 Mendeley Data, V1, doi: 10.17632/53d3ktbg8d.1.

598

599 **References**

600 Cui, R., Zhang, D., Hu, W., Zhao, X., Yan, H., Liu, G., Chen, A., 2023. Nitrogen in soil, manure and  
601 sewage has become a major challenge in controlling nitrate pollution in groundwater around plateau  
602 lakes, Southwest China. *J. Hydrol.* 620, 129541.

603 Dai, H., Zhang, Y., Fang, W., Liu, J., Hong, J., Zou, C., Zhang, J., 2023. Microbial community structural  
604 response to variations in physicochemical features of different aquifers. *Front. Microbiol.* 14,  
605 1025964.

606 Díaz-Cruz, M.S., Barceló, D., 2008. Trace organic chemicals contamination in ground water recharge.  
607 *Chemosphere* 72(3), 333-342.

608 Gibrilla, A., Fianko, J.R., Ganyaglo, S., Adomako, D., Anornu, G., Zakaria, N., 2020. Nitrate  
609 contamination and source apportionment in surface and groundwater in Ghana using dual isotopes  
610 ( $^{15}\text{N}$  and  $^{18}\text{O}\text{-NO}_3$ ) and a Bayesian isotope mixing model. *J. Contam. Hydrol.* 233, 103658.

611 Greenberg, A.E., Trussell, R.R., Clesceri, L.S., Association, A.W.W., 2005. Standard methods for the  
612 examination of water and wastewater : supplement to the sixteenth edition. *American Journal of*  
613 *Public Health & the Nations Health* 56(3), 387.

614 Gutiérrez, M., Biagioni, R.N., Alarcón-Herrera, M.T., Rivas-Lucero, B.A., 2018. An overview of nitrate  
615 sources and operating processes in arid and semiarid aquifer systems. *Sci. Total Environ.* 624, 1513-  
616 1522.

617 Hao, Y., Zheng, T., Liu, L., Li, P., Ma, H., Zheng, Z., Zheng, X., Luo, J., 2025. Occurrence of  
618 dissimilatory nitrate reduction to ammonium (DNRA) in groundwater table fluctuation zones during  
619 dissolved organic nitrogen leaching through unsaturated zone. *J. Hazard. Mater.* 489, 137501.

620 Huang, X., Jin, M., Ma, B., Liang, X., Cao, M., Zhang, J., Zhang, Z., Su, J., 2022. Identifying nitrate  
621 sources and transformation in groundwater in a large subtropical basin under a framework of  
622 groundwater flow systems. *J. Hydrol.* 610, 127943.

623 Ji, X., Shu, L., Chen, W., Chen, Z., Shang, X., Yang, Y., Dahlgren, R.A., Zhang, M., 2022. Nitrate  
624 pollution source apportionment, uncertainty and sensitivity analysis across a rural-urban river  
625 network based on  $\delta^{15}\text{N}/\delta^{18}\text{O}\text{-NO}_3^-$  isotopes and SIAR modeling. *J. Hazard. Mater.* 438, 129480.

626 Kellman, L.M., Hillaire-Marcel, C., 2003. Evaluation of nitrogen isotopes as indicators of nitrate  
627 contamination sources in an agricultural watershed. *Agriculture, ecosystems & environment* 95(1),  
628 87-102.

629 Li, J., Liu, Y., Dai, W., Li, J., Yang, P., Tian, L., Yu, S., Zuo, R., Zhai, Y., Song, W., 2023. Nitrate  
630 attenuation with rising groundwater levels: An integrated assessment using isotope tracers and  
631 microbial signatures. *J. Hydrol.* 624, 129911.

632 Li, S., Chow, R., Su, H., Han, F., Li, Z., 2025. Multiple isotopes and GIS analyses reveal sources and  
633 drivers of nitrate in the Loess Plateau's groundwater. *Environ. Pollut.*, 127022.

634 Liang, X., Zhan, H., Zhang, Y.K., Schilling, K., 2017. Base flow recession from unsaturated - saturated  
635 porous media considering lateral unsaturated discharge and aquifer compressibility. *Water Resour.*

636 Res. 53(9), 7832-7852.

637 Liu, S., Zheng, T., Li, Y., Zheng, X., 2023. A critical review of the central role of microbial regulation  
638 in the nitrogen biogeochemical process: New insights for controlling groundwater nitrogen  
639 contamination. *J. Environ. Manage.* 328, 116959.

640 Liu, W., Du, Y., Qiu, W., Deng, Y., Wang, Y., 2025. Constraints on vertical variability of geogenic  
641 ammonium in multi-layered aquifer systems. *Water Res.* 268, 122639.

642 Liu, Y., Xin, J., Wang, Y., Yang, Z., Liu, S., Zheng, X., 2022. Dual roles of dissolved organic nitrogen  
643 in groundwater nitrogen cycling: nitrate precursor and denitrification promoter. *Sci. Total Environ.*  
644 811, 151375.

645 Ma, J., Liu, H., Tong, L., Wang, Y., Chen, R., Liu, S., Zhao, L., Li, Z., Cai, L., 2019. Relationships  
646 between microbial communities and groundwater chemistry in two pristine confined groundwater  
647 aquifers in central China. *Hydrol. Process.* 33(14), 1993-2005.

648 Mao, H., Wang, G., Liao, F., Shi, Z., Zhang, H., Chen, X., Qiao, Z., Li, B., Bai, Y., 2023. Spatial  
649 variability of source contributions to nitrate in regional groundwater based on the positive matrix  
650 factorization and Bayesian model. *J. Hazard. Mater.* 445, 130569.

651 McDonough, L.K., Andersen, M.S., Behnke, M.I., Rutledge, H., Oudone, P., Meredith, K., O Carroll,  
652 D.M., Santos, I.R., Marjo, C.E., Spencer, R.G., 2022. A new conceptual framework for the  
653 transformation of groundwater dissolved organic matter. *Nat. Commun.* 13(1), 2153.

654 Meng, L., Zuo, R., Wang, J., Yang, J., Teng, Y., Shi, R., Zhai, Y., 2018. Apportionment and evolution  
655 of pollution sources in a typical riverside groundwater resource area using PCA-APCS-MLR model.  
656 *J. Contam. Hydrol.* 218, 70-83.

657 Minet, E.P., Goodhue, R., Meier-Augenstein, W., Kalin, R.M., Fenton, O., Richards, K.G., Coxon, C.E.,  
658 2017. Combining stable isotopes with contamination indicators: a method for improved investigation  
659 of nitrate sources and dynamics in aquifers with mixed nitrogen inputs. *Water Res.* 124, 85-96.

660 Moore, J.W., Semmens, B.X., 2008. Incorporating uncertainty and prior information into stable isotope  
661 mixing models. *Ecol. Lett.* 11(5), 470-480. Niu, X., Jia, X., Yang, X., Wang, J., Wei, X., Wu, L.,  
662 Shao, M., 2022. Tracing the sources and fate of NO<sub>3</sub><sup>-</sup> in the vadose zone-groundwater system of a  
663 thousand-year-cultivated region. *Environ. Sci. Technol.* 56(13), 9335-9345.

664 Picetti, R., Deeney, M., Pastorino, S., Miller, M.R., Shah, A., Leon, D.A., Dangour, A.D., Green, R.,  
665 2022. Nitrate and nitrite contamination in drinking water and cancer risk: A systematic review with  
666 meta-analysis. *Environ. Res.* 210, 112988.

667 Ransom, K.M., Grote, M.N., Deinhard, A., Eppich, G., Kendall, C., Sanborn, M.E., Souders, A.K.,  
668 Wimpenny, J., Yin, Q.Z., Young, M., 2016. Bayesian nitrate source apportionment to individual  
669 groundwater wells in the Central Valley by use of elemental and isotopic tracers. *Water Resour. Res.*  
670 52(7), 5577-5597.

671 Rivett, M.O., Buss, S.R., Morgan, P., Smith, J.W., Bemment, C.D., 2008. Nitrate attenuation in  
672 groundwater: a review of biogeochemical controlling processes. *Water Res.* 42(16), 4215-4232.

673 Romanelli, A., Soto, D.X., Matiatos, I., Martínez, D.E., Esquius, S., 2020. A biological and nitrate  
674 isotopic assessment framework to understand eutrophication in aquatic ecosystems. *Sci. Total*  
675 *Environ.* 715, 136909.

676 Ruan, D., Bian, J., Wang, Y., Wu, J., Gu, Z., 2024. Identification of groundwater pollution sources and  
677 health risk assessment in the Songnen Plain based on PCA-APCS-MLR and trapezoidal fuzzy  
678 number-Monte Carlo stochastic simulation model. *J. Hydrol.* 632, 130897.

679 Schot, P.P., Wassen, M.J., 1993. Calcium concentrations in wetland groundwater in relation to water  
680 sources and soil conditions in the recharge area. *J. Hydrol.* 141(1-4), 197-217.

681 Shu, L., Chen, W., Liu, Y., Shang, X., Yang, Y., Dahlgren, R.A., Chen, Z., Zhang, M., Ji, X., 2024.  
682 Riverine nitrate source identification combining  $\delta^{15}\text{N}/\delta^{18}\text{O}-\text{NO}_3^-$  with  $\Delta^{17}\text{O}-\text{NO}_3^-$  and a  
683 nitrification  $^{15}\text{N}$ -enrichment factor in a drinking water source region. *Sci. Total Environ.* 918,  
684 170617.

685 Thurston, G.D., Spengler, J.D., 1985. A quantitative assessment of source contributions to inhalable  
686 particulate matter pollution in metropolitan Boston. *Atmospheric Environment* (1967) 19(1), 9-25.

687 Wan, Y., Li, R., Yao, K., Peng, C., Wang, W., Li, N., Wang, X., 2024. Bioelectro-barriers prevent nitrate  
688 leaching into groundwater via nitrogen retention. *Water Res.* 249, 120988.

689 Wang, D., Li, P., Yang, N., Yang, C., Zhou, Y., Li, J., 2023. Distribution, sources and main controlling  
690 factors of nitrate in a typical intensive agricultural region, northwestern China: vertical profile  
691 perspectives. *Environ. Res.* 237, 116911.

692 Wong, W.W., Grace, M.R., Cartwright, I., Cook, P.L., 2015. Unravelling the origin and fate of nitrate in  
693 an agricultural–urban coastal aquifer. *Biogeochemistry* 122, 343-360.

694 Xie, L., Li, P., Fida, M., Elumalai, V., 2025. Characteristics and potential health risk of inorganic nitrogen  
695 in phreatic water in the central and southern parts of Yinchuan Plain (Northwest China). *Expo. Health*  
696 17(2), 581-598.

697 Xin, J., Liu, Y., Chen, F., Duan, Y., Wei, G., Zheng, X., Li, M., 2019. The missing nitrogen pieces: A  
698 critical review on the distribution, transformation, and budget of nitrogen in the vadose zone-  
699 groundwater system. *Water Res.* 165, 114977.

700 Xin, J., Wang, Y., Shen, Z., Liu, Y., Wang, H., Zheng, X., 2021. Critical review of measures and decision  
701 support tools for groundwater nitrate management: A surface-to-groundwater profile perspective. *J.*  
702 *Hydrol.* 598, 126386.

703 Yang, L., Han, J., Xue, J., Zeng, L., Shi, J., Wu, L., Jiang, Y., 2013. Nitrate source apportionment in a  
704 subtropical watershed using Bayesian model. *Sci. Total Environ.* 463, 340-347.

705 Yu, L., Zheng, T., Yuan, R., Zheng, X., 2022. APCS-MLR model: a convenient and fast method for  
706 quantitative identification of nitrate pollution sources in groundwater. *J. Environ. Manage.* 314,  
707 115101.

708 Yu, L., Zheng, T., Zheng, X., Hao, Y., Yuan, R., 2020. Nitrate source apportionment in groundwater  
709 using Bayesian isotope mixing model based on nitrogen isotope fractionation. *Sci. Total Environ.*  
710 718, 137242.

711 Zhang, T., Lei, Q., Liu, H., Ding, K., Luo, J., Qiu, W., Ma, Y., Xu, Q., Zhao, Y., Liu, X., 2026. Vertical  
712 migration of multi-source nitrates driven by multiple water inputs in groundwater base on combined  
713 nitrogen-oxygen and hydrogen-oxygen isotopes. *J. Hazard. Mater.*, 141181.